ELSEVIER

Journal of Neuroscience Methods 150 (2006) 150–158

JOURNAL OF NEUROSCIENCE METHODS

www.elsevier.com/locate/jneumeth

Efficient quantification of afferent cochlear ultrastructure using design-based stereology☆

Howard W. Francis[a,*], Alejandro Rivas[a], Mohamed Lehar[a], Yu Saito[a], Peter R. Mouton[c,d], David K. Ryugo[a,b]

[a] *Department of Otolaryngology–Head and Neck Surgery, Johns Hopkins University, 601N. Caroline St., JHOC 6th floor, Baltimore, MD 21205, USA*
[b] *Department of Neuroscience, Johns Hopkins University, Baltimore, MD, USA*
[c] *Department of Gerontology Research Center (NIA-NIH), Johns Hopkins Bayview Campus, Baltimore, MD, USA*
[d] *Department of Stereology Resource Center, Baltimore, MD, USA*

Received 13 April 2005; received in revised form 15 June 2005; accepted 16 June 2005

Abstract

The afferent synapse between the auditory nerve fiber and the inner hair cell (IHC) represents a critical junction for hearing. Elucidation of the structure at this site will help establish the substrate for normal sound encoding as well as pathologic processes associated with hearing dysfunction. Previous applications of unbiased (design-based) stereological principles have expanded our knowledge of neuro-morphological changes evident with the light microscope. Applying these principles at the level of the synapse is a promising morphometric approach for the efficient sampling of large reference spaces with electron microscopy. This study tests the accuracy of using ultra-thin sections at a fixed interval, known as disector pairs, to quantify afferent innervation density. We analyzed the total numbers of afferent terminals, synaptic thickenings, and synaptic bodies associated with each IHC in the C57BL/6J mouse cochlea, and confirmed the accuracy of the stereological approach in comparison to three-dimensional reconstructions of serial alternate sections. The higher sampling efficiency of the disector pair method rapidly increases precision while also reducing the largest source of variability, inter-animal differences. We conclude that ultrastructural quantification of afferent innervation can be accomplished in the cochlea using efficient design-based stereology.

Keywords: Cochlea; Inner hair cell; Afferent innervation; Synapse; Nerve terminal; Ultrastructure; Stereology; Disector principle

1. Introduction

The structural relationship between primary auditory neurons and inner hair cells (IHC) remains unclear, especially with respect to the afferent structure of terminal and synaptic morphology. Discharge characteristics of primary neurons differ according to spontaneous discharge rate, threshold at best frequency, maximum discharge rate, and dynamic range (Kiang et al., 1965; Liberman, 1978). Such variations are relevant to the encoding of specific acoustic features that contribute to the extraction of sounds from noise. The encoding properties of each auditory nerve fiber are hypothesized to be influenced by the morphology of both pre- and post-synaptic structures at the IHC synapse (Krishna, 2002; Sumner et al., 2002). Afferent terminal size, mitochondrial content and synaptic shape in the cat cochlea, for example, are strongly correlated to spontaneous discharge rate and dynamic range of auditory nerve fibers (Liberman, 1980; Liberman, 1982; Merchan-Perez and Liberman, 1996). Similar distributions of physiological response characteristics are found in CBA/J and C57BL/6J mice (Taberner and Liberman, 2005), although morphometric correlates of these properties have not been established.

Deviation from normal innervation patterns in the cochlea likely has functional consequences, analogous to structure–function correlates revealed by quantitative anal-

☆ This work has been presented at the 28th MidWinter Meeting of the Association for Research in Otolaryngology, New Orleans, LA, February, 2005 (abstract #664).

* Corresponding author. Tel.: +1 410 955 1640; fax: +1 410 614 8610.
E-mail address: hfrancis@jhmi.edu (H.W. Francis).

0165-0270/$ – see front matter © 2005 Published by Elsevier B.V.
doi:10.1016/j.jneumeth.2005.06.020

yses of pre- and post-synaptic structure in the central nervous system (Geinisman et al., 1992; Murthy et al., 2001; Schikorski and Stevens, 2001). Cognitive decline in humans (Bertoni-Freddari and Fattoretti, 1989; Bertoni-Freddari et al., 2003) and senescence in laboratory animals (Bertoni-Freddari et al., 1996) are associated with a reduction in cortical synaptic density and increases in synaptic size. Changes in dendritic spine morphology and density are also associated with neurological and psychiatric disease (Blanpied and Ehlers, 2004). Similarly, altered synaptic contacts between afferent terminals and IHCs in the cochlea would be expected to disrupt the discharge properties of auditory nerve fibers, corrupt the encoding process, and ultimately impair hearing.

Traditionally, ultrastructural quantification of cochlear afferents has relied on three-dimensional (3D) reconstructions from serial sections. The time- and labor-intensive nature of these approaches, however, limits the number of samples analyzed within each case, as well as the number of cases analyzed in each animal group. This limitation on statistical power hinders the partitioning of the observed variability into its constituent sources: true biological differences and sampling error. Thus, 3D reconstruction is accurate for the limited regions sampled, but fails to capture the required majority of biological variability for reliable hypothesis testing.

Modern stereological methods combine highly efficient and systematic sampling approaches with assumption- and model-free geometric probes that generate estimates with accuracy comparable to that of 3D reconstruction (Gundersen et al., 1999; Mouton, 2002). A critical advantage of systematic sampling is that the total observed variability (coefficient of variation, CV = S.D./mean) provides a reliable estimate of the true variation in the parameter of interest (e.g., total object number and mean object volume) across the entire reference space (Mouton, 2002; Schmitz and Hof, 2005). The total variability can then be partitioned into biological variation (BV, inter-animal differences) and method error (coefficient of error, CE, or intra-animal differences). This partitioning allows sampling protocols to be optimized for maximum efficiency by focusing time and effort on sampling the source of greatest variation (Gundersen et al., 1999). The application of these efficient and unbiased sampling strategies to ultrastructural quantification could increase statistical power for testing hypotheses while avoiding the most severe sources of stereological bias inherent to assumption- and model-based morphometry.

In this paper we compare and contrast 3D reconstructions and design-based stereology for the determination of IHC innervation density in the mouse cochlea. These two methods were used to assess the total number and density of afferent terminals, synaptic bodies, and synapses in 2–3 month old C57BL/6J mice with normal hearing. Specifically, counts from 3D reconstructions using every other ultra-thin section were compared with stereological estimates using the physical disector approach with progressively larger sampling intervals between disector pairs (DP). The application of these methods to the same set of electron micrographs confirmed the accuracy of disector-based stereological estimates. Furthermore, the empirical data from stereology estimates established a basis for the development of an optimally efficient sampling protocol to quantify age- and disease-related morphological changes of IHC innervation that affect normal hearing.

1.1. Relevant principles of design-based stereology

The goal of 3D reconstruction using serial or semi-serial sections is to count all objects of interest within the anatomically defined volume of tissue (reference space). By comparison, the goal of design-based stereology is to make reliable estimates using unbiased geometric probes, e.g., DP's, placed at systematic random locations through the reference space. With continued sampling through the reference space, both methods lead to the same result — reliable quantification of the objects of biological interest.

Unbiased estimates of object number require a 3D geometric probe called a disector that renders the same sampling probability (i.e., $P = 1$) to each object of interest regardless of object size, shape, or orientation relative to the plane of sectioning (Sterio, 1984; Mouton, 2002; Schmitz and Hof, 2005). In the present application, one DP consists of two adjacent ultra-thin sections a known distance, h, apart (h = disector height). The optimal distance between the reference and look-up sections is less than the minimum caliper height of objects of interest, which prevents undercounting should these objects fall between the two planes of the DP. Objects are counted that are present within one section (reference section) but not the other (look-up) section. This approach allows the user to identify the "tops" of each object contained within a known volume of tissue. Since each object contains only one top-most point regardless of size, shape, or orientation relative to the plane of sectioning, this approach provides an unbiased estimate of numerical density, i.e., number of objects per unit volume, without further assumptions.

Disector pairs are evenly (systematically) distributed within the reference volume after randomly selecting the first DP. Using the fractionator method of sampling (Gundersen, 1986), objects are counted in a known fraction of the total reference volume, and estimates of total object number are calculated as the product of the number of objects counted $\left(\sum Q^{-}\right)$ and the reciprocal of the volume fraction analyzed. As the number of DP's at systematic random locations through the reference volume increases, variability due to sampling error [coefficient of error (CE)] decreases, causing the estimate to converge on the true value. The rate at which the sampling error declines as a function of increased sampling provides the basis for the high efficiency of systematic random sampling: The CE decreases as a direct linear function of the number (n) of disectors counted, i.e., $CE = 1/n$, compared to $1/\sqrt{n}$ for purely random (independent) sampling (Stuart, 1976). It has been shown that the most efficient strategy for rapidly capturing the variability in an estimate is to set the CE to about one-half or less of the biological variability

(BV) (Gundersen et al., 1999). This approach ensures that the sampling error (CE) makes a relatively minor contribution to the overall variation, and focuses effort on reducing the larger source of variance (BV) by studying more animals. Thus, an important attribute of stereological sampling is efficiency-convergence on the true value with a minimum of time and effort (Gundersen and Østerby, 1981).

2. Materials and methods

2.1. Animals

Five 2–3 month old C57BL/6J mice with normal hearing were studied in accordance with an animal protocol approved by the Animal Care and Use Committee at the Johns Hopkins University School of Medicine. As detailed below, morphological correlates of afferent innervation to IHCs (numbers of afferent terminals, synaptic membrane specializations and synaptic bodies) were counted in three animals using 3D reconstruction methods applied to alternate serial sections of transmission electron micrographs through IHCs. Using the same set of images, estimates of these structural parameters were made using the disector principle and systematic random sampling (Mouton, 2002). To assess the contribution of sampling error to parameter estimates, additional studies were carried out with increasing sampling intervals between DP's for five mice.

2.2. Tissue preparation and microscopy

Sampling was carried out at 55% distance from the cochlear apex in all animals, a location corresponding to 22 kHz (Rivas et al., 2005; Muller et al., 2005). As previously described, the cochleae were harvested to minimize effects of hypoxia on afferent terminal structure, and prepared for both light and electron microscopy (Hequembourg and Liberman, 2001; Francis et al., 2003, 2004). In brief, each animal was deeply anesthetized with intraperitoneal administration (5 ml/kg, I.P.) of ketamine (25 mg/ml), xylazine (2.5 mg/ml) and ethanol (14.25%), and in vivo perfusion of one cochlea was performed with 1% OsO_4/1% potassium ferricyanide (KFeCN) in a fume hood. The animal was euthanized and the head submerged in the same fixative for an additional 45 min after which the cochlea was removed. Following decalcification with 0.1 M EDTA (with 1% glutaraldehyde), the cochlea was dehydrated in graded alcohols and propylene oxide, and then embedded in Araldite. The cochlea was sectioned parallel to the modiolus at 40 μm thickness and mounted between sheets of Aclar for light microscopic analysis and reconstruction. Digital light micrographs of all sections were aligned with a PC application called *Serial EM* (*sEM*) available online at http://synapses.bu.edu/, using the absolute mode (Falia and Harris, 2001a). The junction of inner and outer pillars was traced in series to create a 3D spiral along the organ of Corti. The segment of the organ of Corti located 55% distance from the apex was embedded in Epon and cut perpendicular to the long axis of the IHC at a thickness of 75 nm. Ultra-thin sections were placed in series on Formvar grids and stained with uranyl acetate. Electron micrographs were taken using a Jeol JEM-100CX II microscope at 60 kV at 2700 magnification for every other section below the IHC nucleus, digitized and aligned with *sEM* using supporting cell nuclei as fiduciary landmarks. Aligned sections were imported into *Neurolucida* (Microbrightfield Inc., Essex, VT) where IHCs, nerve terminals, and synaptic bodies were outlined, and synaptic membrane specializations were traced. Average section thickness was determined separately for each block of tissue using the minimal folds method applied to random sections (De Groot, 1988; Falia and Harris, 2001b).

2.3. Three-dimensional analysis of serial alternate sections

Three-dimensional reconstruction of serial alternate sections was done in three mice, which served as the gold standard for comparison with stereological methods. Individual terminals were identified based on the continuity of profiles between sections and the identification of their upper and lower limits. As previously described in the mouse cochlea (Sobkowicz et al., 1986), the synaptic membrane specialization was defined as an electron dense asymmetric thickening of opposed membranes, whereas the electron dense synaptic body (SB) was found in the pre-synaptic region within the IHC and was surrounded by a halo of clear vesicles (Fig. 1). The number of afferent terminals, synaptic membrane specializations and synaptic bodies per IHC were tallied as their

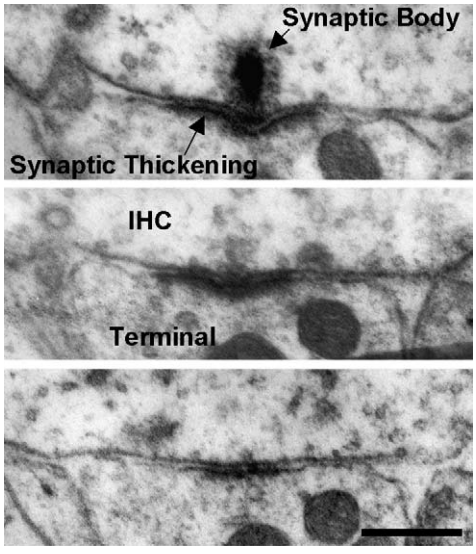

Fig. 1. Transmission electron micrographs of three adjacent sections showing the ultrastructural features that are counted to determine the afferent innervation density of IHCs: asymmetric membrane thickening characteristic of the afferent synapse, the electron dense synaptic body in the pre-synaptic region of the IHC, and the apposition between the IHC and the afferent nerve terminal. Scale bar = 0.25 μm.

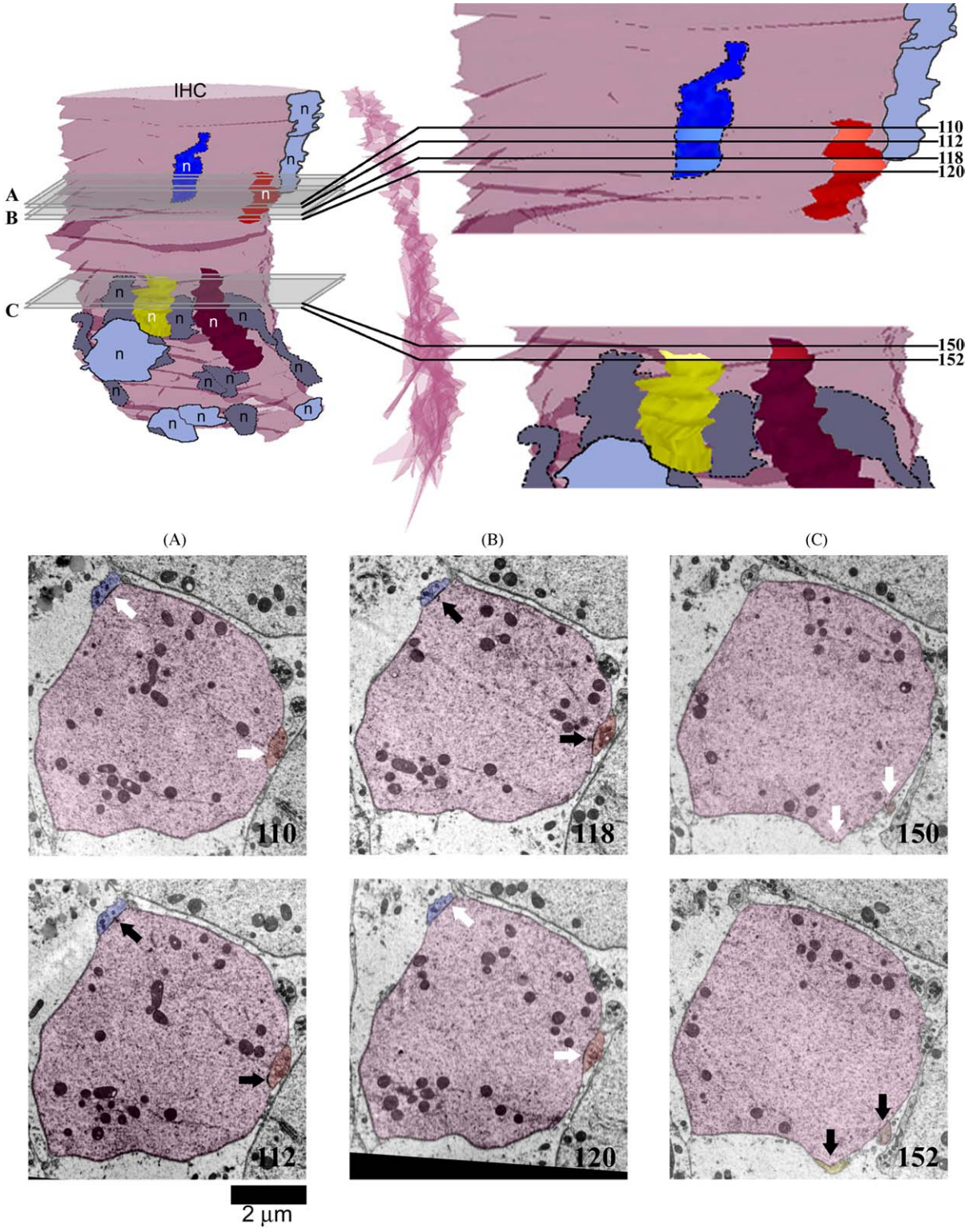

Fig. 2. Whereas afferent structures in the infra-nuclear region are counted as whole objects following 3D reconstruction of the IHC and afferent terminals (upper panel), only their edges are counted by disector pair sampling (lower panel). The position of disector pairs A–C are shown in the 3D reconstruction of an IHC created using serial alternate sections. Terminals are labeled "*n*", with those located on the far surface of the hair cell distinguished by dark grey filling and a broken outline. Four reconstructed terminals are color-coded to facilitate comparison with the transmission electron micrographs below. Objects are counted when present in the reference section (black arrows) and absent in the look-up section (white arrows), such as (A) synaptic thickening and a synaptic body (B) two synaptic bodies, and (C) two nerve terminal appositions with the IHC. Scale bar = 2 µm.

upper and lower limits were encountered, and confirmed using the 3D reconstruction of traced profiles made by *NeuroExplorer* (Microbrightfield Inc., Essex, VT).

2.4. Analysis of disector pairs

Objects were counted that fell within the unbiased counting frame on the reference section (Fig. 2A–C, black arrow) but did not appear on the look-up section (white arrow). The entire reference space was contained within each section, therefore counting frames to avoid edge effects and sub-sampling of areas within each section were not required (area sampling fraction = 1). Repetition of this sampling procedure using a known fraction of sections through the reference volume (V_R), generated a true count of the number of objects $\left(\sum Q^-_{obj}\right)$ in the corresponding volume fraction. The section sampling fraction (ssf) was calculated as the total thickness of DP's used (H_{dp}) divided by the thickness of the reference space (H_R), i.e., the fraction of all possible DP's. For the present study the reference space was unambiguously defined as the volume of IHC between the inferior section of the nucleus and the inferior pole of the cell.

Transmission electron micrographs were digitized, aligned and organized into DP's separated by a single section starting randomly at the inferior pole of the IHC nucleus (Fig. 2). Nerve terminals were counted when an apposition occurred along the IHC in the reference section, but not the look-up section (Fig. 2C); and, synaptic membrane thickening and synaptic bodies were counted when present in the reference section, but absent in the look-up section (Fig. 2A and B). The interval between both sections of the DP was determined by the caliper length of the smallest object of interest, i.e., the synaptic body. It was determined that the size of synaptic bodies (Fig. 3) requires a maximum of one ultra-thin section between sections in the DP to ensure that no synaptic bodies could fall between them.

The numbers of terminal appositions, synaptic membrane thickenings and synaptic bodies were counted for 3–5 IHCs per cochlea. Counts were repeated by reversing the roles of the reference and look-up sections in the DP's and were averaged into a mean sum (mean $\sum Q^-_{obj}$). For each object of interest with known values for $\sum Q^-_{obj}$, H_{dp}, and H_R, calculation of total number of objects, N_{obj} follows from the relationship:

$$N_{obj} = \sum Q^-_{obj}(F_1)(F_2)$$

where, F_1 = 1/ssf = V_R/V_{dp} = H_R/H_{dp}, F_2 = 1/tsf = 1/thickness sampling fraction = 1, tsf = disector height/section thickness = 3/3 = 1, disector height = distance between outer surfaces of two sections in each disector pair = 3, section thickness = thickness of tissue sampled by each disector pair = 3.

The thickness sampling fraction is most relevant in light microscopic studies of thick sections using optical disectors, in which the disector pair height, or distance between focal planes, is a fraction of the section thickness. In the current study the disector height (three sections) is equivalent to the tissue thickness that is being examined (three sections); therefore, F_2 equals 1.

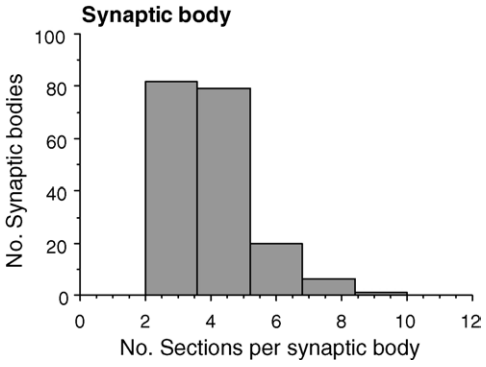

Fig. 3. The maximum allowable distance between disector pairs is determined by the smallest diameter of the synaptic body, the smallest object of interest. The diameter of individual synaptic bodies found in 11 IHCs located 55% distance from the cochlear apex in three 2–3 month old mice, is presented as the number of sections in which they are present. A disector pair separated by one section should be small enough to capture even the smallest synaptic body within the tissue thickness sampled. A disector height of three sections is therefore selected for this study based on this analysis of the smallest object of interest.

3. Results

The analysis of sections using the physical disector approach is equivalent to traditional 3D reconstruction or serial analysis of the same sections. Whether arranged as single sections in series for analysis by 3D reconstruction or arranged as disector pairs with a height of three sections one section apart (Fig. 4A), comparable numbers of afferent structures per IHC (Fig. 4B) are counted in a single cochlea using the same series of alternate sections. Mean numbers of synaptic thickenings and nerve terminals per IHC determined using 3D reconstruction (*x*-axis) were within one standard deviation of estimates using DP's (*y*-axis). The mean number of synaptic bodies and synaptic thickenings per IHC estimated using DP's were within one standard deviation of results of 3D reconstruction. It is therefore feasible to obtain an accurate estimate of afferent innervation density in the mouse cochlea by applying the physical disector method using a disector height of 3, or a pair of sections separated by one section. We then analyzed the precision and efficiency of estimates at the same cochlear location as a function of sampling interval in a group of 2–3 month old animals.

Relative to 3D reconstructions, the physical disector method generated comparable estimates of afferent innervation density over a wide range of sampling intervals (Fig. 5). Fig. 5 shows the central tendency (mean+/−S.D.) and individual differences for estimates of the number per IHC of synaptic thickenings (Fig. 5A), synaptic bodies (Fig. 5B), and nerve terminals (Fig. 5C) by 3D reconstruction in three an-

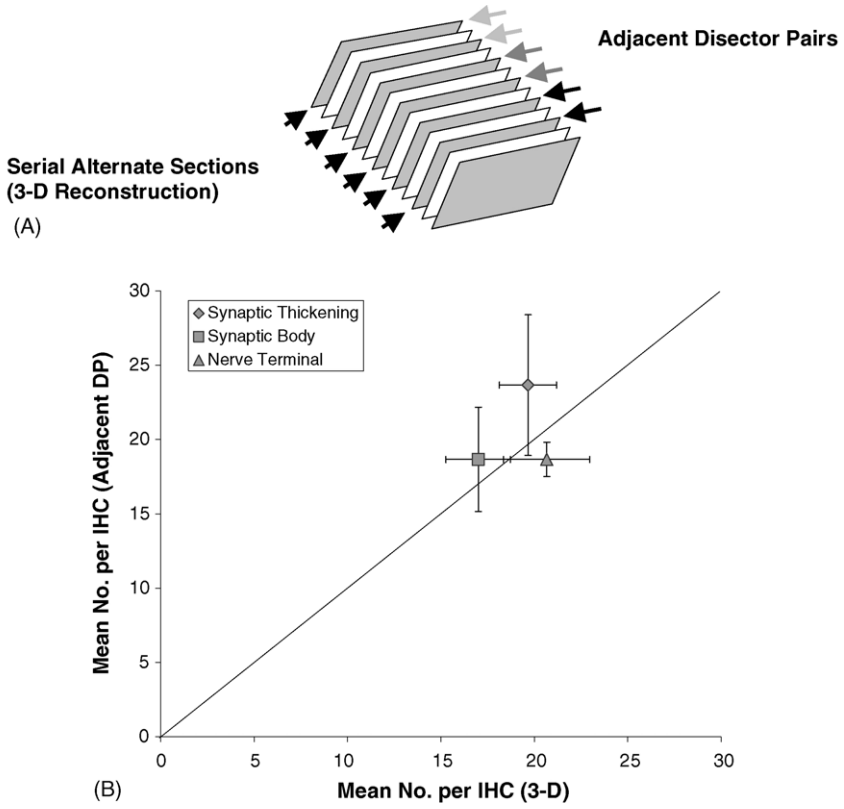

Fig. 4. Estimates of afferent innervation density using disector pairs are comparable to the results of 3D reconstruction in a single cochlea. Whether the same stack of alternate sections (shaded grey) is analyzed in series by 3D reconstruction or as disector pairs separated by a single section (A), similar mean numbers of synaptic thickenings, synaptic bodies and terminal appositions per IHC are obtained for three IHCs (B). DP: disector pair.

imals (16.8 ± 3.2, 15.7 ± 2.5, $17.23 \pm .5$, respectively), and by DP's separated by 5, 13, 29 and 61 sections. There were no significant differences across disector pair intervals or between estimates resulting from DP and 3D reconstruction methods (ANOVA, $p > .05$) for estimates of mean number of synaptic thickening, synaptic body and nerve terminals per IHC.

As expected, sampling error (CE) was lowest for 3D reconstruction and increased as a direct function of sampling interval (Table 1). Despite these increases in within-animal variability, differences between animals (BV) remained the dominant source of variability, accounting for over 90% of the total variation in the number of synaptic thickenings per IHC for all sampling intervals (Table 1). Similar trends were observed for the variance of synaptic body and nerve terminal data.

As shown in Table 2, a stable mean estimate for total number of synaptic thickenings is more efficiently achieved using the disector pair method, and increasingly so as the interval between DP's widens. Therefore, as time is spent sampling more cells and animals the rate of convergence of data to the true mean is faster for larger than smaller DP intervals. For 3D reconstruction sampling error is reduced at a rate of 0.34 ($\times 10^{-3}$), compared to rates of 9.45 ($\times 10^{-3}$) for DP's separated by 13 sections, and 65.64 ($\times 10^{-3}$) for DP's separated by 61 sections. Every unit of effort is therefore associated with larger reductions in variability and greater improvements in statistical power for wider relative to narrower DP intervals.

Table 1
Sources of variability in estimates of the number of synaptic thickenings per IHC

	3D reconstruction	Disector pair intervals (sections)			
	SAS	5	13	29	61
CV	0.188	0.32	0.4	0.52	0.769
CE	0.022	0.035	0.090	0.144	0.312
BV = $\sqrt{(CV^2 - CE^2)}$	0.187	0.318	0.390	0.497	0.703
(BV/CV) × 100	99.3	99.4	97.5	96.05	91.4

SAS: serial alternate sections; CV: coefficient of variance (S.D./mean); CE: coefficient of error (CV/$\sqrt{N}$, where N is average number of DP's analyzed); BV: biological variability.

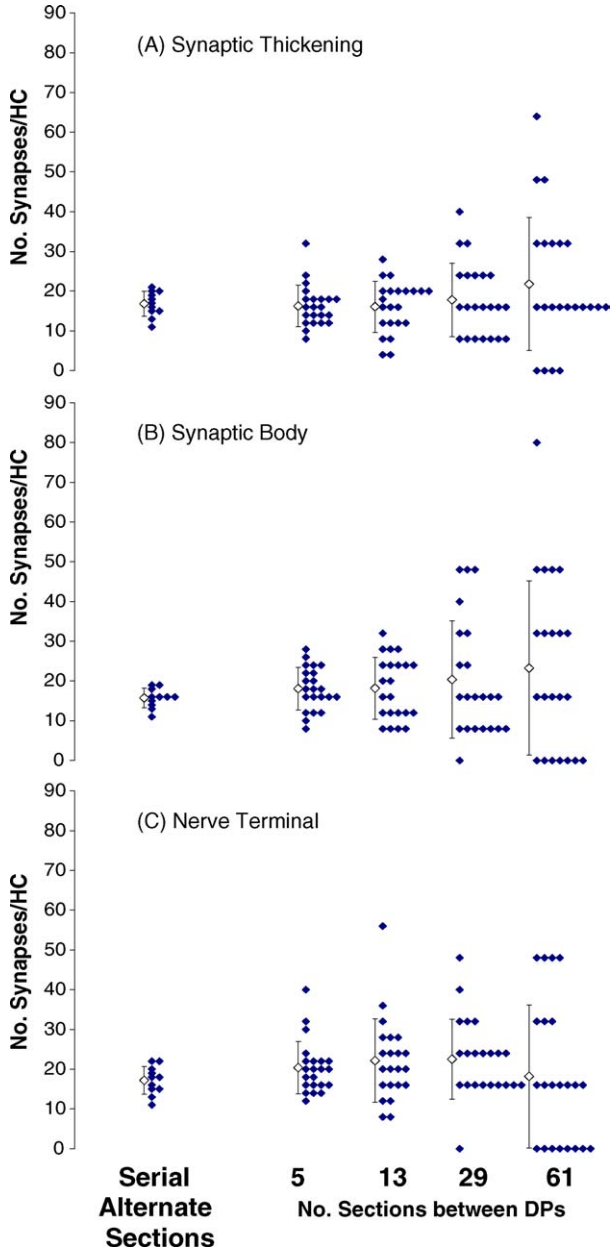

Fig. 5. Mean estimates of the number of (A) synaptic thickenings, (B) synaptic bodies and (C) nerve terminals per IHC using disector pairs separated by increasing sampling intervals are comparable to results of 3D reconstruction of serial alternate sections (ANOVA, $p > .05$ for all measures). Disector pair sampling was conducted in five animals whereas 3D reconstruction was performed in three of them, all at 55% distance from cochlear apex.

4. Discussion

Quantitative analysis of IHC innervation in this study was focused on well-defined afferent structures, the further study of which may provide a valuable foundation for understanding their functional correlates. No morphometric studies to date have attempted to correlate age- or other disease-related deficiencies with pathologic changes at the IHC afferent synapse. One reason for a lack of progress in this area is the reliance on precise, but extremely time-consuming 3D reconstruction methods that prevent sampling of an adequate number of regions and individuals to support hypothesis testing.

The present study demonstrates that accurate estimates of numbers of nerve terminals and synaptic structures per IHC can be obtained using the disector principle. These estimates remain stable at increasing intervals between disector pairs while achieving higher levels of sampling efficiency. These findings, therefore, support stereological analysis of ultrastructural images as an accurate and efficient methodology for the morphometric study of cochlear innervation for studies of normal hearing, aging, hearing disorders and the therapeutic management of disease.

We conducted 3D reconstructions of serial alternate sections in three mice as a standard against which the accuracy and precision of the disector pair principle (Sterio, 1984) could be compared. The relationship between sampling error (CE, a measure of within-sample precision) and time spent on a morphometric study provides a basis for making relative comparisons of the efficiency of different sampling schemes. Table 2 indicates the relatively low efficiency of determining the total number of synaptic thickenings by the 3D reconstruction method, 0.38 ($\times 10^{-3}$), which reflects an average time of 65 h to analyze 80–90 sections for each cochlea. In contrast, an average of 9.5 h was required to estimate the same parameter to a comparable level of accuracy using DP's spaced 13 sections apart, a 25–30-fold increase in efficiency (0.38 versus 10.1). Expanding the DP interval to 29 sections revealed an even larger improvement in efficiency – over 150-fold (0.38 versus 64.2) – without a marked change in the accuracy of the estimate. Thus, these findings confirm that stereological sampling strongly improves efficiency while achieving accuracy that is comparable to 3D reconstruction.

Although accurate in the regions analyzed, traditional methods of serial section reconstruction in a few animals lack

Table 2
Comparison of efficiency for the determination of number of synaptic thickenings per IHC using 3D reconstruction and disector pair sampling of increasing intervals

	3D reconstruction	Disector pair intervals (sections)			
	(SAS)	5	13	29	61
No. of animals	3	5	5	5	5
Mean no. sections/IHC	83.7	39.9	20.4	10.8	5.7
Time per IHC (hours)	65	19	9.5	6.3	4.75
Efficiency (CE)/$t(\times 10^{-3})$	0.34	1.82	9.45	22.83	65.64

SAS: serial alternate sections; CE: coefficient of error.

the statistical power to overcome the major obstacle to hypothesis testing. Stereological approaches that use systematic random sampling enable the partitioning of overall variability into the major sources of error, which in turn allows the investigator to efficiently reduce the major source of variation in morphometric data. An optimally efficient experimental design progressively reduces the observed variation in the data by relatively light sampling within each reference space. This strategy avoids over sampling for little to no gain and conserves time and effort for sampling a sufficient number of individuals to reveal group differences in the parameter of interest.

Total observed variation (CV) for estimates of numbers of synaptic thickenings per IHC (Table 1), as well as synaptic bodies and nerve endings (data not shown), can be partitioned into biological variability (BV) and sampling error (CE) for the purposes of selecting the optimally efficient sampling scheme. For determinations of total object number using 3D reconstruction of serial alternate sections (far left, Fig. 5A), the average number of synapse thickenings varies in the range of 10–20 per IHC, revealing an expected or true value for the inter-animal differences of about 19% (BV = 0.19). Since the total amount of observed variability in this parameter is the same (CV = 0.19), we can conclude that the total variability in this estimate arises from biological differences between IHCs and individual mice. It would therefore be inefficient and wasteful to further reduce the sampling error since biological differences between animals account for the vast majority of the variation in the results and need to be addressed in order to achieve the necessary statistical power for hypothesis testing. Here we show that a more efficient strategy is to reduce the effort required per animal by increasing the sampling interval to 13 sections (CE = 0.10), which is 25–30 times more efficient than 3D reconstruction, and then spend the dividend in time and resources to increase the statistical power by analyzing more animals selected at random from the population. In this case, the increased time and effort directly reduces the major source of variation in the results — biological differences.

These preliminary studies provide a guide for subsequent studies to test biologically relevant hypotheses. For group comparisons, the most efficient strategy would allow the highest amount of variability in control and experimental groups that reveals a significant difference between mean values ($p < 0.05$). For example, disease or treatment effects that cause 50% or more change in the number of synaptic thickenings per IHC relative to controls (Fig. 5A), may be statistically discernible using DP sampling intervals of up to 29 sections. In this case, the combination of DP's and systematic random sampling would reject the null hypothesis using only a small fraction of the time and effort per IHC relative to 3D reconstruction, while allowing for the study of an adequate sample of animals ($n = 5$).

This report provides baseline information on the number of nerve terminals, synaptic thickenings and synaptic bodies that compose the afferent innervation of IHCs at the 22 kHz location in young C57BL/6J mice with normal hearing (Table 1). We have previously observed that each afferent terminal in the C57BL/6J mouse produces a single afferent membrane specialization composed of asymmetric thickening of apposed membranes and a synaptic body in about 85% of cases (Francis et al., 2004). There was no significant difference however between the number of synaptic bodies and synaptic thickenings for either the 3D reconstruction or DP analysis in this study. The mean number of afferent terminals and synaptic structures are comparable to innervation densities estimated in NMR1 mice (7–19 endings/IHC) using light microscopic assessment of fiber density and IHC counts (Ehret, 1979). Ultrastructural studies of afferent innervation of IHCs conducted in other animals report densities ((Francis et al., 2004), Table 2) that are comparable to those observed in the current study, although the influence of cochlear location on these values is not fully known. The number of terminals per IHC was determined to be 15–17 in the third turn and 25–27 in the basal region in adult guinea pig (Hashimoto et al., 1990), 22–30 per IHC in the adult cat (Liberman, 1980, 1982; Liberman et al., 1990; Merchan-Perez and Liberman, 1996), and 15–20 terminals per IHC in the apex and 21–25 in the base for the gerbil (Slepecky et al., 2000).

5. Conclusions

This ultrastructural study of morphological correlates for afferent innervation of IHCs in mouse cochlea confirms the accuracy of stereological sampling using DP's with that of 3D reconstruction. Second, a "cost versus benefit" analysis demonstrates the strong advantage of efficient stereological sampling using the DP's over relatively time- and labor-intensive determinations by 3D reconstruction. Although the results in this study derive from the analysis of synaptic structures in mouse cochlea, the principles are entirely general and can be applied to the optimization of sampling for analyses of other structures at the ultrastructural level.

Acknowledgements

This work was supported by NIH grants DC000143, DC00232, DC05211 and DC05909, and grants from the American Hearing Research Foundation, Deafness Research Foundation and National Organization for Hearing Research. Thanks to Sarah Lehar and Anna Lunn for their contributions to the work presented here.

References

Bertoni-Freddari C, Fattoretti P. Computer-assisted morphometry of synaptic plasticity during aging and dementia. Path Res Pract 1989;185:799–802.

Bertoni-Freddari C, Fattoretti P, Paoloni R, Caselli U, et al. Synaptic structural dynamics and aging. Gerontology 1996;42:170–80.

Bertoni-Freddari C, Fattoretti P, Solazzi M, Giorgetti B, et al. Neuronal death versus synaptic pathology in Alzheimer's disease. Ann NY Acad Sci 2003;1010:635–8.

Blanpied TA, Ehlers MD. Microanatomy of dendritic spines: emerging principles of synaptic pathology in psychiatric and neurological disease. Biol Psychiat 2004;55(12):1121–7.

De Groot DMG. Comparison of methods for estimation of the thickness of ultrathin tissue sections. J Microscopy 1988;151(1):23–42.

Ehret G. Quantitative analysis of nerve fibre densities in the cochlea of the house mouse (*Mus musculus*). J Comp Neurol 1979;183:73–88.

Falia JC, Harris KM. Cylindrical diameters method for calibrating section thickness in serial electron microscopy. J Microsc 2001a;202(3):468–72.

Falia JC, Harris KM. Extending unbiased stereology of brain ultrastructure to three-dimensional volumes. J Am Med Inform Assoc 2001b;8(1):1–16.

Francis HW, Rivas A, Lehar M, Ryugo DK. Two types of afferent terminals innervate cochlear inner hair cells in C57BL/6J mice. Brain Res 2004;1016(2):182–94.

Francis HW, Ryugo DK, Gorelikow MJ, Prosen CA, et al. The functional age of hearing loss in a mouse model of presbycusis. Part II. Neuroanatomical correlates. Hear Res 2003;183(1/2):29–36.

Geinisman Y, de Toledo-Morrell L, Morrell F, Persina I, et al. Structural synaptic plasticity associated with the induction of long-term potentiation is preserved in the dentate gyrus of aged rats. Hippocampus 1992;2(4):445–56.

Gundersen H. Stereology of arbitrary particles: a review of number and size estimators, and the presentation of some new ones, in memory of William R. Thompson. J Microsc 1986;143:3–45.

Gundersen H, Jensen E, Kieu K, Nielsen J. The efficiency of systematic sampling in stereology — revisited. J Microsc 1999;193:199–211.

Gundersen H, Østerby R. Optimizing sampling efficiency of stereological studies in biology: or "Do more less well". J Microsc 1981;121:65–73.

Hashimoto S, Kimura RS, Takasaka T. Computer-aided three-dimensional reconstruction of the inner hair cells and their nerve endings in the guinea pig cochlea. Acta Oto-laryngol (Stockh) 1990;109:228–34.

Hequembourg S, Liberman MC. Spiral ligament pathology: a major aspect of age-related cochlear degeneration in C57BL/6 mice. JARO 2001;2:118–29.

Kiang NY-S, Watanabe T, Thomas EC, Clark LF. Discharge patterns of single fibers in the cat's auditory nerve. Cambridge: MIT Press; 1965.

Krishna BS. A unified mechanism for spontaneous-rate and first-spike timing in the auditory nerve. J Comput Neurosci 2002;13:71–91.

Liberman MC. Auditory-nerve response from cats raised in a low-noise chamber. J Acoust Soc Am 1978;63:442–55.

Liberman MC. Morphological differences among radial afferent fibers in the cat cochlea: an electron-microscopic study of serial sections. Hear Res 1980;3:45–63.

Liberman MC. Single-neuron labeling in the cat auditory nerve. Science 1982;216:1239–41.

Liberman MC, Dodds LW, Pierce S. Afferent and efferent innervaton of the cat cochlea: quantitative analysis with light and electron microscopy. J Comp Neurol 1990;301:443–60.

Merchan-Perez A, Liberman MC. Ultrastructural differences among afferent synapses on cochlear hair cells: correlations with spontaneous discharge rate. J Comp Neurol 1996;371(2):208–21.

Mouton PR. Principles and practices of unbiased stereology: an introduction for bioscientists. Baltimore: Johns Hopkins University Press; 2002.

Muller M, von Hunerbein K, Hoidis S, Smolders JWT. A physiological place-frequency map of the cochlea in the CBA/J mouse. Hear Res 2005;202:63–73.

Murthy VN, Schikorski T, Stevens CF, Zhu Y. Inactivity produces increases in neurotransmitter release and synapse size. Neuron 2001;32(4):673–82.

Rivas A, Montey K, Muniak M, Ryugo DK, et al. Cochlear frequency map of the CBA/J mouse: an anatomical and physiological study. In: 28th Annual Midwinter Meeting of the Association for Research in Otolaryngology; 2005, abstract 596.

Schikorski T, Stevens CF. Morphological correlates of functionally defined synaptic vesicle populations. Nat Neurosci 2001;4(4):391–5.

Schmitz C, Hof P. Design-based stereology in neuroscience. Neuroscience 2005;130:813–31.

Slepecky NB, Galsky MD, Swartzentruber-Martin H, Savage J. Study of afferent nerve terminals and fibers in the gerbil cochlea: distribution by size. Hear Res 2000;144:124–34.

Sobkowicz HM, Rose JE, Scott GL, Levenick CV. Distribution of synaptic ribbons in the developing organ of Corti. J Neurocytol 1986;15(6):693–714.

Sterio DC. The unbiased estimation of numbers and sizes of arbitrary particles using the disector. J Microsc 1984;134:127–36.

Stuart A. The ideas of sampling. 3rd ed. New York: Oxford University Press; 1976.

Sumner CJ, Lopez-Poveda EA, O'Mard LP, Meddis R. A revised model of the inner-hair cell and auditory-nerve complex. J Acoust Soc Am 2002;111(5):2178–88.

Taberner AM, Liberman MC. Response properties of single auditory nerve fibers in the mouse. J Neurophysiol 2005;93(1):557–69.